International Journal of GEOMATE, June., 2021, Vol.20, Issue 82, pp.132-139
ISSN: 2186-2982 (P), 2186-2990 (O), Japan, DOI: https://doi.org/10.21660/2021.82.Gx409
Geotechnique, Construction Materials and Environment

NUMERICAL ANALYSIS OF INVASION PATTERNS DURING DRAINAGE PROCESS IN A SIMPLIFIED PORE NETWORK MODEL

*Yuto Takeuchi[1], Junichiro Takeuchi[2] and Masayuki Fujihara[3]

[1,2,3] Graduate School of Agriculture, Kyoto University, Japan

*Corresponding Author, Received: 25 Nov. 2020, Revised: 27 Feb. 2021, Accepted: 08 Mar. 2021

ABSTRACT: Immiscible two-phase flows in porous media is of concern for various problems such as underground water pollution by non-aqueous phase liquid and enhanced oil recovery. It is understood that the drainage process in porous media exhibits patterns of either stable displacement, viscous fingering flow or capillary fingering flow depending on the conditions. However, the physical mechanism of the invasion and critical conditions for different invasion patterns have not been universally identified. This study employed a numerical two-phase flow simulation using the Color Gradient Lattice Boltzmann Method (CG-LBM) in a simplified pore network model with different capillary numbers and viscosity ratios between the two fluids. Simulation results confirm that flows for a low capillary number produce the preferential flow for pores with the least threshold pressure, which corresponds to capillary fingering flow. In addition, the retreat of the invading fluid caused by the Haines jump was observed. When the capillary number is higher, these two phenomena were not observed. Flows with a higher capillary number lead the invading fluid to simultaneously displace different pores when its viscosity is higher than that of the invaded fluid (stable displacement), and the viscous fingering flow happens otherwise. These findings suggest that capillary number and viscosity ratio, and occurrence of the preferential flow and Haines jump are key factors that determine invasion patterns.

Keywords: Fingering flow, Lattice Boltzmann Method, Drainage process, Capillary number

1. INTRODUCTION

Immiscible two-phase flows in porous media is of concern for various problems such as underground water pollution by non-aqueous phase liquid, enhanced oil recovery, and carbon capture and storage. The drainage process in porous media exhibits various patterns depending on conditions namely from the stable displacement, viscous fingering flow to capillary fingering flow. Although the critical conditions determining these invasion patterns have been widely researched both physically [1–3] and numerically [4–6], there is no universally accepted criteria regarding the transition among the different invasion patterns. In addition, the detailed physical mechanism during fluid displacement in porous media has not been explicitly identified.

One of the most influential works about the drainage process in porous media was conducted by Lenormand et al. [7]. They numerically simulated displacement behavior by a capillary network model and classified the invasion patterns based on the saturation when breakthrough occurs. In their study, the results were presented as a phase diagram which has the viscosity ratio (M) on the x-axis and the capillary number (Ca) on the y-axis, and the type of invasion patterns are plotted accordingly. Although their work successfully reproduced different invasion patterns and classified them, it is reported that the threshold of the diagram is not universally fixed [1, 3, 5]. Also, it lacks analyses of the detailed process during displacement because it assumes simple capillary network fluid dynamics.

This paper numerically simulates the drainage process within a simplified pore network model using the Color Gradient Lattice Boltzmann Method (CG-LBM) with different conditions of Ca and M. The numerical results confirmed the three invasion patterns depending on the conditions, and the two notable fluid dynamic phenomena, the preferential flow and Haines jump, were observed, which were considered as key factors for different invasion patterns.

2. MATERIALS AND METHODS

2.1 Numerical Scheme

The Lattice Boltzmann Method (LBM) is a mesoscopic-based computational fluid method and treats a fluid as a collection of particles which have discretized lattice velocities. The probability of particles heading to a certain direction at a node is described by the particle distribution function. Fluid properties such as density, pressure and velocity are derived by the zeroth and first moment of the particle distribution function. The computational

procedure of the standard LBM consists of two steps: the collision and streaming steps. The simple iteration of these two steps develops the particle distribution functions. Further, the computation of the moments of the particle distribution functions yields macroscopic variables at each node so that it recovers the incompressible Navier-Stokes equation within the limit of low Mach number [8].

The CG-LBM is a multiphase LBM model that is effective at explicit specification of fluid properties such as the viscosity ratio and interfacial tension. We implemented a computational method mainly based on [9], where multiphase features of interfacial tension and immiscibility were incorporated by adding a perturbation step and recoloring step to the standard LBM procedure, respectively. Fluid wettability was modelled by directly assigning the contact angle without considering the contact angle hysteresis [10].

Regarding boundary conditions, the standard bounce-back condition was applied at the walls of the porous model as the no-slip boundary condition, and the non-equilibrium bounce back method [11] was utilized at the inlet and outlet boundary as the Dirichlet boundary condition.

The computer code we used was verified beforehand by simulating basic multiphase flow problems of the droplet formation and contact angle test (not shown), and satisfactory results were obtained. Throughout the simulations in this research, the contact angle of the wetting fluid against the nonwetting fluid was set at 60 degrees.

2.2 Simulation Outline

Considering the high computational cost of the CG-LBM, a simplified pore network model was chosen as the simulated medium. The simulated porous model shown in Fig. 1 is composed of four circular pore bodies with the same size, four rectangular throats connecting them with different widths, and inlet and outlet throats. The widths w of the pore throats and diameter d of the pore bodies are presented in Table 1 as a dimensionless lattice unit (lu). Note that all the values are non-dimensionalized using lattice unit (lu), mass unit (mu), and time step (ts) for length, mass, and time unit, respectively, in the rest of the paper. Constant velocity was imposed at the inlet, and constant pressure was imposed at the outlet. The inlet boundary nodes are assumed to be nonwetting nodes, and the outlet boundary nodes were assumed to be wetting nodes. The inlet velocity drives the red nonwetting fluid to invade the pores and the blue wetting fluid is drained from the outlet.

The key parameters of the simulation were capillary number $Ca = \mu_n u_n / \sigma$ and viscosity ratio $M = \mu_n / \mu_w$. Note that μ_n is the dynamic viscosity of the nonwetting fluid, u_n is the inlet velocity of the nonwetting fluid, σ is the interfacial tension, and μ_w is the dynamic viscosity of the wetting fluid. Several works about the drainage process in porous media [1, 3, 5, 7] showed that the stable displacement occurs when both Ca and M are higher, the viscous fingering flow occurs when Ca is higher and M is lower, and capillary fingering flow occurs when Ca is lower. However, the thresholds of the transition among those invasion patterns are different among different studies, and hence a universal criterion has not been established. In addition, the physical mechanism of the different invasion patterns has not been adequately researched because of the complexity of porous media.

We changed the two parameters of Ca and M by appropriately choosing the kinematic viscosity, fluid density, interfacial tension, and inlet velocity from simulation to simulation while keeping the LBM specific error due to large velocity and kinematic viscosity small. Indeed, the maximum inlet velocity allowed was set as 0.009 and that of the kinematic viscosity to be 0.6. We realized the capillary number ranged from $Ca = 5.0 \times 10^{-5}$ to 7.2×10^{-2} and the viscosity ratio $M = 9.000$ and 0.111. The simulation was stopped when the invading fluid reached the outlet of the medium, i.e., when breakthrough occurs. The simulation results exhibit different invasion patterns each of which corresponds to the stable displacement, viscous fingering flow and capillary fingering flow. The physical mechanisms of the various displacement processes and their transitions are analyzed in the next section.

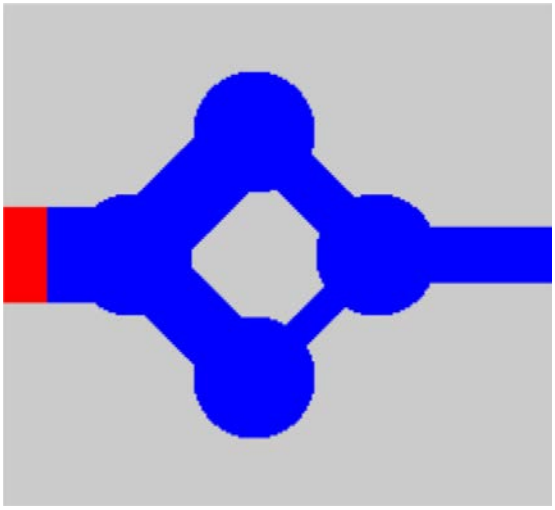

Fig. 1 The simulated porous model. The red region is occupied by an invading fluid and the blue region is occupied by an invaded fluid.

Table 1 Widths w of the pore throats and radius d of the pore bodies in the simulated porous model

w_{BL}	w_{TL}	w_{BR}	w_{TR}	d_B	w_I	w_O
84	96	36	60	150	120	72

Note: BL: Bottom-Left, TL: Top-Left, BR: Bottom-Right, TR: Top-Right, B: Body, I: Inlet, O: Outlet. The unit is lattice unit (lu).

3. RESULTS AND DISCUSSION

3.1 Capillary Fingering Flow

The representative flow development for the capillary fingering pattern is shown in Fig. 2. This regime assumes a lower capillary number, and therefore the flow is dominated by capillary force while the viscosity effect is negligible.

The first notable characteristic is the preferential flow to the larger pore throats. As Fig. 2a shows, the invading fluid preferentially invades the top left throat without entering the bottom left throat. This phenomenon is caused by variant threshold pressures of the pore throats. The threshold pressure of a throat is defined as the pressure difference between the two fluids needed for the invading fluid to invade the throat. In the drainage process, according to the Laplace law, the threshold pressure P^{th} is written as

$$P^{th} = \frac{2\sigma\cos\theta}{w}, \tag{1}$$

where θ is the contact angle measured in the invaded wetting fluid. Since the contact angle and interfacial tension are constants, wider throats always hold smaller threshold pressure, leading the invading fluid to invade wider throats preferentially. While the fluid invades the pore throat with the largest throat width, the pressure difference between the invading and invaded fluid is fixed to the threshold pressure of that throat which is inevitably lower than the threshold pressure of the other pore throat. Hence, the invading fluid is not able to invade the other throat, and waits at the entrance of the throat (Fig. 2a).

In addition, another preferential pattern between a pore body and throat is noticeable. From Fig. 2a to Fig. 2b, the invading fluid prefers the bottom left throat rather than the top body. The threshold pressure into pore bodies can be computed by the Laplace law and geometrical calculation following a similar method to Xu et al. [10]. The schematic figure for the derivation of the threshold pressure into round pore bodies is shown in Fig. 3. The symbols R, α, and θ_{app} in Fig. 3 denote the radius of curvature of the fluid interface, angle between the pore throat and pore body wall, and apparent contact angle, respectively. The angle α is determined only by the geometry of the porous model, and $\cos\alpha = -w/d$ and $90° < \alpha < 180°$ hold. Although the apparent contact angle is equal to the fluid contact angle θ while invading the pore throat, it undergoes an abrupt increase when reaching the pore body. When reaching the pore body, the meniscus swells while sticking to the critical points of the throat-body, and the apparent contact angle declines until it becomes equal to the fluid contact angle θ [10]. When it becomes equal to the fluid contact angle θ, the invasion of the pore body starts and the meniscus moves into the pore body. Considering the relationship of the angles in Fig. 3, the radius of curvature R is calculated by

$$R = -\frac{w}{2\cos(\alpha + \theta_{app})}, \tag{2}$$

and hence the pressure difference is

$$\Delta P = -\frac{2\sigma\cos(\alpha + \theta_{app})}{w}. \tag{3}$$

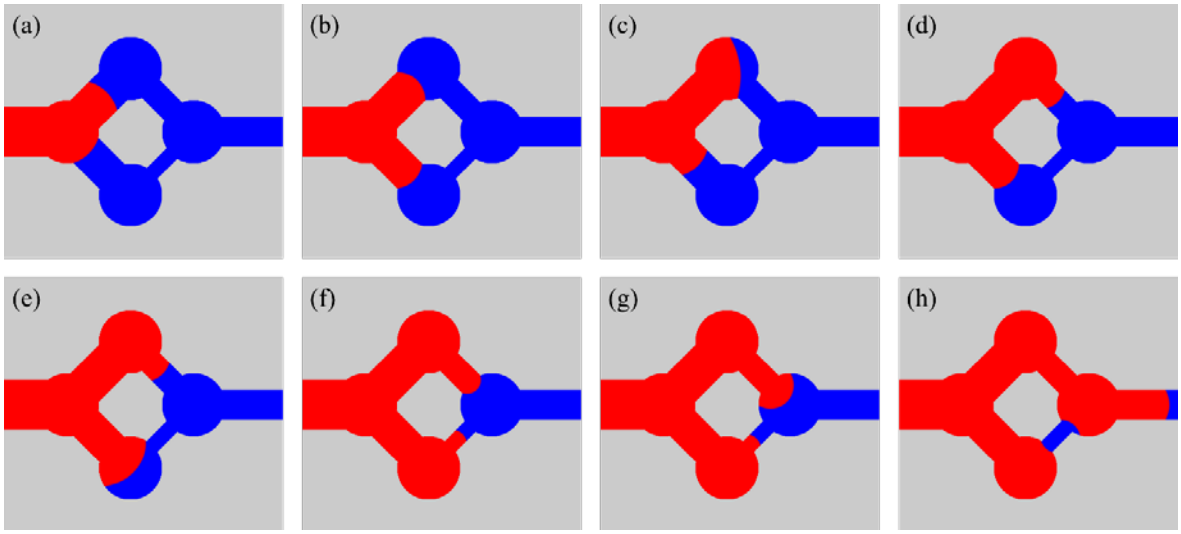

Fig. 2 The representative flow development in capillary fingering regime ($Ca = 3.6\times10^{-4}$, $M = 9.000$).

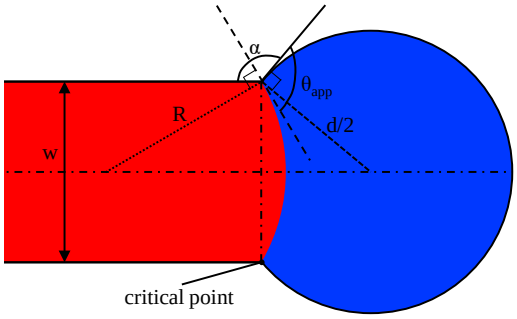

Fig. 3 Schematic figure of invasion from pore throat to pore body

When $\alpha+\theta \le 180°$, the maximum pressure difference is encountered when $\alpha+\theta_{app}=180°$. When $\alpha+\theta \ge 180°$, the invasion starts before $\alpha+\theta_{app}$ becomes 180°, and thus the maximum pressure difference occurs when $\alpha+\theta_{app}=\alpha+\theta$. Therefore the threshold pressure into a pore body with diameter d from a throat with width w is:

$$P^{th} = -\frac{2\sigma\cos[\max(\alpha+\theta, 180^{\circ})]}{w}. \quad (4)$$

The threshold pressure into the top body from the top left throat is thus $P^{th} = -2\sigma\cos(\alpha+\theta)/96 \approx 0.021\sigma$, which is higher than the threshold pressure into the bottom left throat $P^{th} = 2\sigma\cos 60°/84 \approx 0.012\sigma$. Hence, the invading fluid invades the bottom left throat rather than the top body (Fig. 2b). Then, the invading fluid enters the top body rather than the bottom body, following Eq. (4) (Fig. 2c).

During the invasion of the top body, the second characteristic, or the retreat of the invading fluid from the throat due to the Haines jump [12] occurs. Haines jump is an abrupt increase and decrease in fluid interface and pressure, respectively [12]. When the invading fluid invades the top body from the top left throat, the invading fluid undergoes the sudden change in geometry and an accompanying sudden drop in capillary pressure. This makes the pressure of the invading fluid less than the pressure needed to stay in the bottom left throat. Hence, the invading fluid in the bottom left throat retreats, and the redistribution of the fluid occurs.

The difference between the average pressure of the invading and invaded fluids, and the average x-velocity before and during the invasion of the top pore body are plotted in Fig. 4 for the same condition as Fig. 2. During period (A), the invading fluid invades the bottom left throat, keeping a constant pressure. Then, during period (B), the pressure starts to increase by growing the menisci while the interfaces stick to the critical points between the top left throat and top body, and the bottom left throat and bottom body. Finally it releases the pressure during the period (C) while invading the top body. Accompanying to the sharp pressure decline, the invading fluid retreats from the bottom left throat from (D) to (E).

Also, the average x-velocity experiences an abrupt increase and decrease during the retreat. This jump and retreat event happened in a short period (~660,000 time steps) compared to the initial invasion of the bottom left throat (~120,000 time steps). The average x-velocity presented in Fig. 4 also illustrates the rapidness of the jump and retreat. This process is typical of the Haines jump phenomenon: accumulation of pressure, abrupt exchange of pressure into velocity, and fluid redistribution.

After refilling the bottom left throat in accordance with Eq. (1), the invading fluid invades the top right throat as a result of comparison

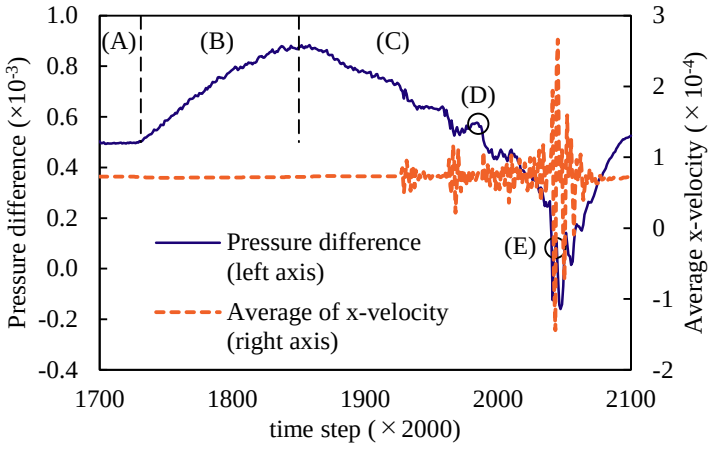

Fig. 4 Pressure difference and average x-velocity about invasion of top body. (A) Invade bottom left throat. (B) Accumulate pressure by growing menisci while sticking to critical points. (C) Invade top body while releasing pressure. (D) Start to retreat from bottom left throat. (E) Retreat completely to reach left body

between Eq. (1) for the top right throat and Eq. (4) for the bottom body (Fig. 2d). Then, the bottom body is invaded while the Haines jump occurs (Fig. 2e) after which the top right throat is refilled. The threshold pressure into the right body $P^{th} = -2\sigma\cos(180°)/60 = \sigma/30$ is higher than that into the bottom right throat $P^{th} = 2\sigma\cos(60°)/36 = \sigma/36$. Hence, the bottom right throat is invaded rather than the right body (Fig. 2f). Interestingly, the meniscus between the top right throat and right body (Fig. 2f) swells more than those between the left body and bottom left throat (Fig. 2a) and between the bottom left throat and bottom body (Fig. 2d). Since the threshold pressure into the bottom right throat is relatively higher and close to that into the right body, the pressure difference had to be increased by growing the meniscus and decreasing the apparent contact angle to enter the bottom right throat before Fig. 2f (see Eq. (3) and Fig. 3). After the displacement in the bottom right throat, the Haines jump occurs while invading the right body (Fig. 2g), and the breakthrough occurs (Fig. 2h).

3.2 Stable Displacement

The representative flow development for the stable displacement pattern is shown in Fig. 5. In this regime, the capillary number is higher, and the viscosity ratio is larger. Hence, the viscosity of the invading fluid is dominant. In this regime the preferential flow and Haines jump mentioned in the capillary fingering pattern were not observed. On the contrary, the invading fluid simultaneously invades the bottom left throat and the top left throat (Fig. 5a). In this case, the dominant viscous force of the invading fluid diminishes the local capillary effect due to the interfacial tension, i.e., the threshold pressure does not affect the propagation of the meniscus lying in the other throat. The retreat of the invading fluid due to the Haines jump does not take place for the same reason: during the displacement of a large pore body, the invading fluid is still able to displace the invaded fluid, propelled by the bulk pressure difference (Fig. 5b, c, d, e).

3.3 Viscous Fingering Flow

The representative flow development for the viscous fingering pattern is shown in Fig. 6. This regime had a higher capillary number and smaller

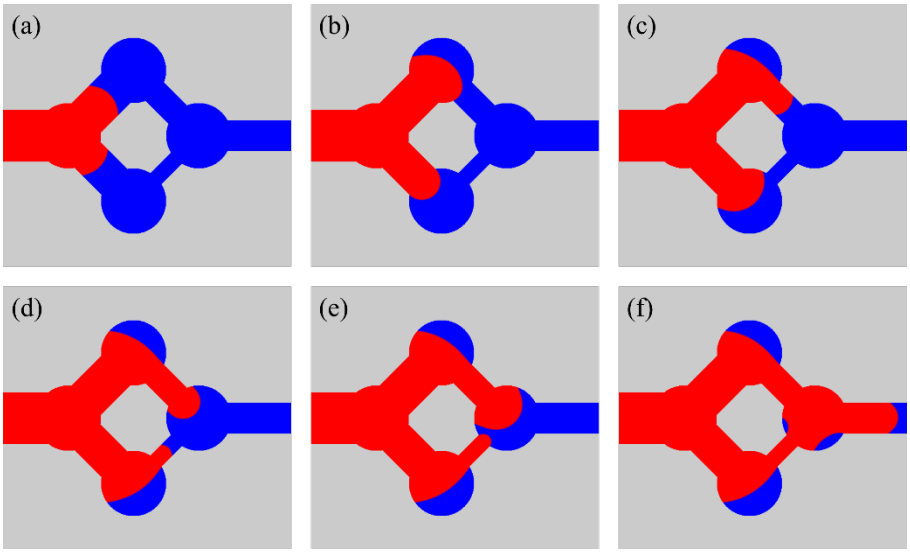

Fig. 5 The representative flow development in stable displacement regime ($Ca = 7.2\times10^{-2}$, $M = 9.000$).

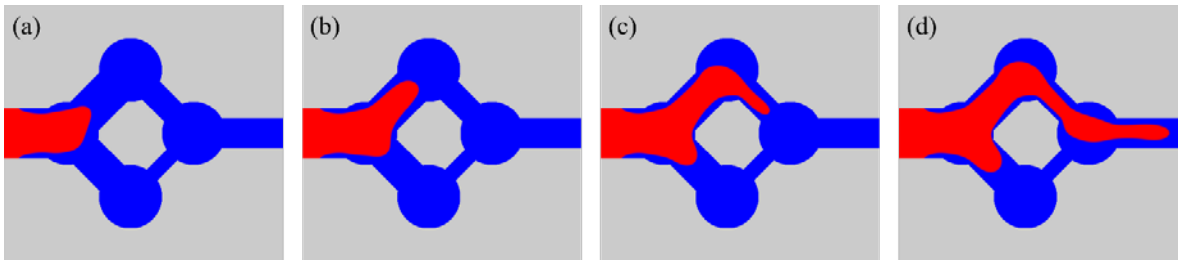

Fig. 6 The representative flow development in viscous fingering regime ($Ca = 7.2\times10^{-2}$, $M = 0.111$).

viscosity ratio. Hence, the flow is dominated by the viscosity of the invaded fluid. In this flow type, the finger-like interface is confirmed. As with the stable displacement pattern, the flow is driven by the bulk pressure difference between the inlet and outlet, and therefore the capillarity of the pores does not affect the fluid dynamics. Observing the state at breakthrough (Fig. 6d), the seemingly preferential path to the upper pores is evident, which is not by the capillarity but rather by the channeling effect [13, 14]. In the viscous fingering pattern, since bulk pressure difference is much larger than the local capillary pressure difference, the pore selection of invasion does not occur pore by pore unlike the capillary fingering pattern. Instead, the overall viscous resistance through the series of pores from the inlet to the outlet determines the flow path. In this manner, the upper series of pores is preferable for the invading fluid compared to the lower one. In other words, the upper channel is more permeable than the lower channel.

3.4 Transition Among Different Flow Patterns

The critical values for the transition among the three invasion patterns are of interest from an engineering viewpoint because the different invasion patterns significantly alter the efficiency of the operation. Tables 2 and 3 show the presence and absence of the noted phenomena in the capillary fingering regime, the preferential flow and retreat of the invading fluid due to Haines jump, for different viscosity ratios. From Table 2, the capillary fingering flow would transition to the stable displacement in capillary number on the order of 10^{-2}, which roughly corresponds to [3] and [7]. Table 3 suggests that the transition from the capillary fingering to the viscous fingering would occur in capillary number on the order of 10^{-3}, which is considerably higher than that reported in some of the literature [1, 3]. Since the domain size significantly influences the invasion patterns, simulation on larger realistic porous media is needed for further analysis.

To further understand the mechanisms of the invasion patterns the transitional capillary numbers should be investigated as the interplay between viscosity and capillarity occurs in those conditions. In reality, the drainage process in natural porous media cannot be easily distinguished among the three invasion patterns, and the several patterns coexist simultaneously [6]: both the viscosity and capillarity take effect in realistic conditions.

Figure 7 shows the flow development for $Ca = 1.0 \times 10^{-2}$ and $M = 9.000$, equivalent to the transitional pattern from the capillary fingering flow to the stable displacement. In this condition, the preferential flow and retreat due to the Haines jump was weak. The invading fluid invaded multiple pores simultaneously, but primarily selected the pore with the smaller threshold pressure (Fig. 7a). Further, the invading fluid retreated from the pore throats due to the Haines jump, but the retreat was incomplete. The moderate retreat from the bottom left throat was evident between Fig. 7b and c. As shown in Fig. 7d to e, the top right pore throat and bottom pore body were simultaneously displaced, which was not observed in the capillary fingering flow (Fig. 2). Nevertheless, a retreat from the top right throat occurred, as seen in Fig. 7f, likely due to the Haines jump. This indicates that the characteristic phenomenon of the capillary

Table 2 Presence and absence of preferential flow and retreat by Haines jump when $M = 9.000$

Ca	5.0 $\times10^{-5}$	1.0 $\times10^{-4}$	3.6 $\times10^{-4}$	3.6 $\times10^{-3}$	7.2 $\times10^{-3}$	1.0 $\times10^{-2}$	2.0 $\times10^{-2}$	3.6 $\times10^{-2}$	7.2 $\times10^{-2}$
logCa	-4.30	-4.00	-3.44	-2.44	-2.14	-2.00	-1.70	-1.44	-1.14
Preferential flow	Present	Present	Present	Present	Intermediate	Intermediate	Absent	Absent	Absent
Retreat by Haines jump	Present	Present	Present	Present	Present	Present	Intermediate	Absent	Absent

Table 3 Presence and absence of preferential flow and retreat by Haines jump when $M = 0.111$

Ca	5.0 $\times10^{-5}$	1.0 $\times10^{-4}$	3.6 $\times10^{-4}$	7.2 $\times10^{-4}$	3.6 $\times10^{-3}$	7.2 $\times10^{-3}$	1.0 $\times10^{-2}$	3.6 $\times10^{-2}$	7.2× 10^{-2}
logCa	-4.30	-4.00	-3.44	-3.14	-2.44	-2.14	-2.00	-1.44	-1.14
Preferential flow	Present	Present	Intermediate	Absent	Absent	Absent	Absent	Absent	Absent
Retreat by Haines jump	Present	Present	Present	Present	Intermediate	Absent	Absent	Absent	Absent

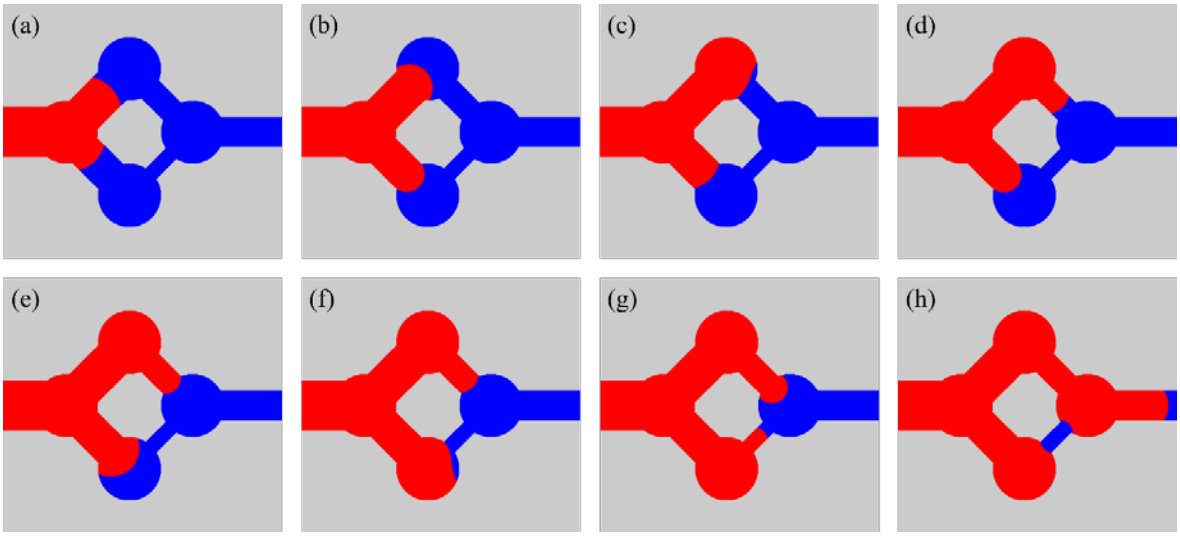

Fig. 7 Flow development for $Ca = 1.0 \times 10^{-2}$, $M = 9.000$.

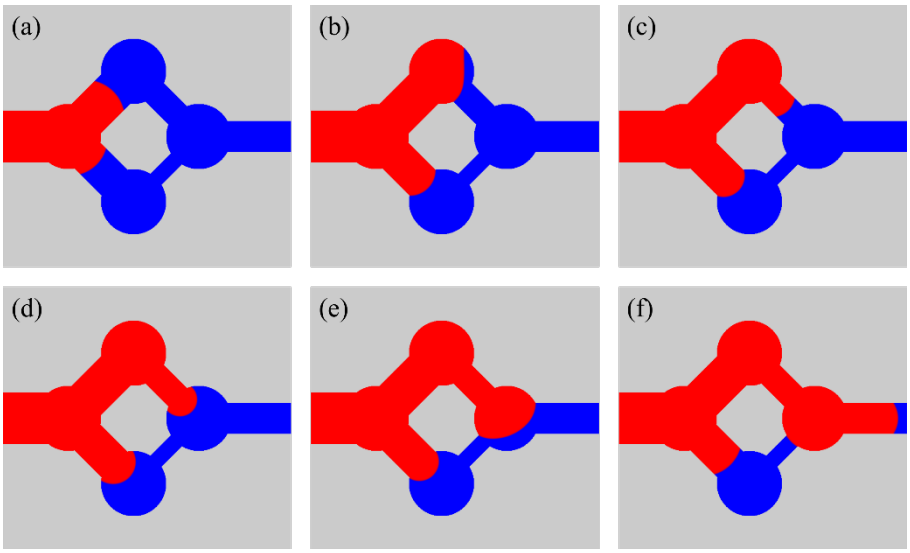

Fig. 8 Flow development for $Ca = 7.2 \times 10^{-4}$, $M = 0.111$.

fingering flow did still exist. Overall, this pattern highlights the interplay between the viscosity and capillarity.

Figure 8 shows the flow development for $Ca = 7.2 \times 10^{-4}$ and $M = 0.111$, corresponding to the transitional pattern from the capillary fingering flow to the viscous fingering flow. As presented in Fig. 8a, the top left and bottom left throats were simultaneously displaced although more dominantly for the top left throat. This pattern is same as $Ca = 1.0 \times 10^{-2}$ and $M = 9.000$ (Fig. 7a). In addition, as shown in Fig. 8a to Fig. 8b, the top pore body and bottom left pore throat were simultaneously displaced. In Fig. 8c, it can be observed that the invading fluid chose to invade the top right throat rather than the bottom pore body, which is the same selection as the capillary fingering flow pattern and in accordance with the comparison of the threshold pressures. However, an alternative interpretation is possible: the invading fluid evades the bottom channel composing of the narrow bottom right throat. This theory is based on the discussion of the viscous fingering flow pattern, in which we proposed that the invading fluid selects the series of the pores with smaller viscous resistance. After filling the top right throat, the bottom and right body were simultaneously displaced (Fig. 8d), after which the invading fluid retreated from the bottom body as the right body continued to be invaded (Fig. 8e). At the breakthrough (Fig. 8f), the retreated fluid even reached the inside of the bottom left throat. The pattern in Fig. 8 again demonstrates the interplay between viscosity and capillarity. Further substantial work is required to explore the

theoretical argument about transitional flow patterns.

4. CONCLUSIONS

In this paper, the drainage process in a simplified pore network model was numerically simulated using the CG-LBM, and the three different invasion patterns were obtained. These patterns correspond to the capillary fingering flow, stable displacement, and viscous fingering flow. Two phenomena were observed for low capillary number flows (i) the preferential flow to the pores with the least threshold pressure and (ii) the retreat of the invading fluid due to the Haines jump. During the Haines jump, a sudden release of pressure and an abrupt change in mean velocity were observed. Whereas, the preferential flow and Haines jump were not observed for higher capillary number flows. When Ca is larger than the order of 10^{-2} and $\mu_n / \mu_w = 9.000$, the pore throats were simultaneously displaced, which corresponds to stable displacement. When Ca is larger than the order of 10^{-3} and $\mu_n / \mu_w = 0.111$, the viscous fingering flow developed, where the finger-like interface was observed. These findings suggest that the conditions of capillary number and viscosity ratio, and occurrence of the preferential flow and Haines jump are key factors that determine different invasion patterns.

5. ACKNOWLEDGMENTS

This work was supported by JSPS KAKENHI Grant Number JP 20H03100.

6. REFERENCES

[1] Chen Y. F., Wu D. S., Fang S., and Hu R., Experimental study on two-phase flow in rough fracture: Phase diagram and localized flow channel. International Journal of Heat and Mass Transfer, Vol. 122, 2018, pp.1298-1307.

[2] Ferer M., Ji C., Bromhal G. S., Cook J., Ahmadi G., and Smith D. H., Crossover from capillary fingering to viscous fingering for immiscible unstable flow: Experiment and modeling. Physical Review E, Vol. 70, Issue 1, 2004, 016303.

[3] Zhang C., Oostrom M., Wietsma, T. W., Grate J. W., and Warner, M. G., Influence of viscous and capillary forces on immiscible fluid displacement: Pore-scale experimental study in a water-wet micromodel demonstrating viscous and capillary fingering. Energy & Fuels, Vol. 25, Issue 8, 2011, pp.3493-3505.

[4] Chen Y., Li Y., Valocchi A. J., and Christensen K. T., Lattice Boltzmann simulations of liquid CO2 displacing water in a 2D heterogeneous micromodel at reservoir pressure conditions. Journal of Contaminant Hydrology, Vol. 212, 2018, pp.14-27.

[5] Liu H., Zhang Y., and Valocchi A. J., Lattice Boltzmann simulation of immiscible fluid displacement in porous media: Homogeneous versus heterogeneous pore network. Physics of Fluids, Vol. 27, Issue 5, 2015, 052103.

[6] Tsuji T., Jiang F., and Christensen K. T., Characterization of immiscible fluid displacement processes with various capillary numbers and viscosity ratios in 3D natural sandstone. Advances in Water Resources, Vol. 95, 2016, pp.3-15.

[7] Lenormand R., Touboul E., and Zarcone C., Numerical models and experiments on immiscible displacements in porous media. Journal of Fluid Mechanics, Vol. 189, 1988, pp.165-187.

[8] Krüger T., Kusumaatmaja H., Kuzmin A., Shardt O., Silva G., and Viggen E. M.. The lattice Boltzmann method. Springer International Publishing, 2017.

[9] Leclaire S., Pellerin N., Reggio M., and Trépanier J. Y., Enhanced equilibrium distribution functions for simulating immiscible multiphase flows with variable density ratios in a class of lattice Boltzmann models. International Journal of Multiphase Flow, Vol. 57, 2013, pp.159-168.

[10] Xu Z., Liu H., and Valocchi A. J., Lattice Boltzmann simulation of immiscible two-phase flow with capillary valve effect in porous media. Water Resources Research, Vol. 53, Issue 5, 2017, pp.3770-3790.

[11] Zou Q., and He X., On pressure and velocity boundary conditions for the lattice Boltzmann BGK model. Physics of Fluids, Vol. 9, Issue 6, 1997, pp.1591-1598.

[12] Sun Z., and Santamarina J. C., Haines jumps: Pore scale mechanisms. Physical Review E, Vol. 100, Issue 2, 2019, 023115.

[13] Tsang C. F., and Neretnieks I., Flow channeling in heterogeneous fractured rocks. Reviews of Geophysics, Vol. 36, Issue 2, 1998, pp.275-298.

[14] Tang Y. B., Li M., Bernabé Y., and Zhao J. Z., Viscous Fingering and Preferential Flow Paths in Heterogeneous Porous Media. Journal of Geophysical Research: Solid Earth, Vol. 125, Issue 3, 2020, e2019JB019